Supporting Information for

A family of mechanically adaptive supramolecular graphene oxide/poly(ethylenimine) hydrogels from aqueous assembly†

Chao Wang‡, Yipin Duan‡, Nicole S. Zacharia* and Bryan D. Vogt*

Department of Polymer Engineering, University of Akron, Akron, OH 44325

* nzacharia@uakron.edu and vogt@uakron.edu

As the oxidation of graphene in the modified Hummers method is stochastic, there is potential for some batch to batch variation in the oxygen content and functional groups on the GO. A second batch of GO (denoted as GO-2) was synthesized and compared with the GO reported throughout the manuscript (hereafter denoted as GO-1). If the GO batch is not denoted in the description, this will be associated with GO-1. The characteristics of the GO were determined by titration, Fig. S1(a) and S1(b), and zeta potential measurements. For titration, the Gran plot was used to determine the equilibrium point.[1, 2] The Gran functions (G) are described by Equation (1) and (2).

$$\text{At acid side: } G_a = (V_{GO} + V_{NaOH}) \times 10^{-pH} \times 100 \quad (1)$$

$$\text{At base side: } G_b = (V_{GO} + V_{NaOH}) \times 10^{-(14-pH)} \times 100 \quad (2)$$

where V_{GO} is the initial volume of GO solution; V_{NaOH} is the volume of NaOH added into the system. Two equilibrium points (V_{EP1}, V_{EP2}) can be obtained by fitting the linear region of the curve, Fig. S1(c) and S1(d), where the equilibrium points are the intersects of the fitted line and the x-axis. The first point is attributed to the carboxylic groups and the second is attributed to the

phenolic groups.[3] The concentration of the carboxylic groups and phenolic groups (mmol/g) on the GO can be calculated by Equation (3) and (4).

$$H_{carboxylic} = \frac{V_{EP1} \times c_{NaOH}}{m_{GO}} \quad (3)$$

$$H_{phenolic} = \frac{(V_{EP2} - V_{EP1}) \times c_{NaOH}}{m_{GO}} \quad (4)$$

where c_{NaOH} is the concentration of the NaOH solution, and m_{GO} is the mass of GO in the titation.

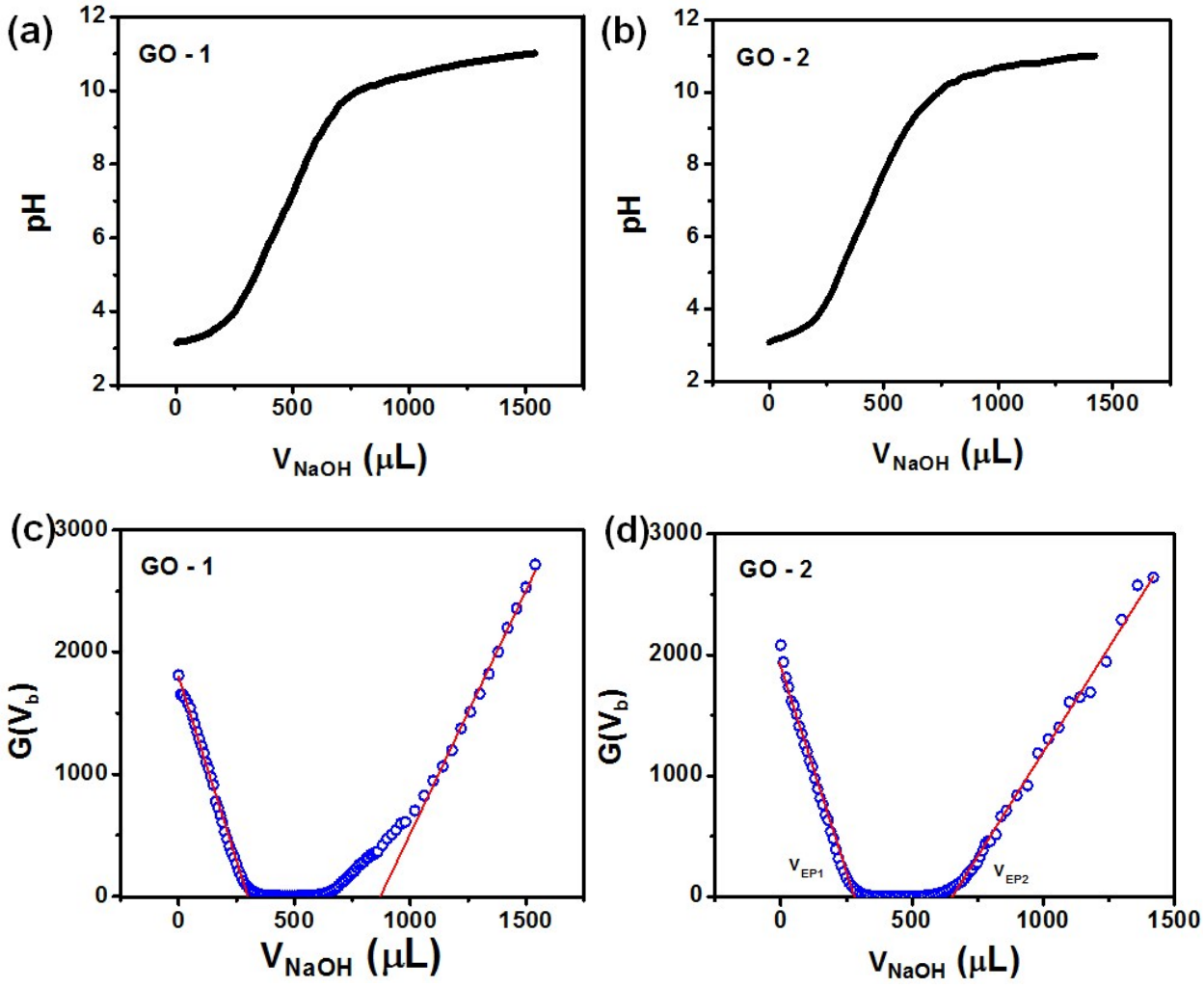

Fig. S1 (a) (b) The GO titration curves. (c) (d) Gran plots obtained from titration data.

Table. S1 shows the batch-to-batch variation in GO synthesized by improved Hummer's method. GO - 1 shows a higher concentration of functional groups. Consequently, it has a larger absolute value of Zeta potential at pH = 2.80.

Table S1. The concentrations of the functional groups on GO and zeta potential of GO at pH = 2.80.

Sample ID	$H_{carboxylic}$ (mmol / g)	$H_{phenolic}$ (mmol / g)	Zeta Potential at pH=2.80 (mV)
GO - 1	1.35	2.32	-33.3 ± 1.5
GO - 2	1.22	1.62	-27.2 ± 1.5

Fig. S2a and S2b illustrate the TGA curves of the dried GO/BPEI hydrogels. The curves exhibit 3 stages. Initially on heating from 30 to 120 °C, there is a gradual weight loss of 5-15 %, which is attributed to removal of unbounded water as it is difficult to fully dehydrate BPEI.[4] A large decrease in mass is observed on further heating, which is associated with the pyrolysis of the oxygen-containing functional groups in GO. For sufficiently high [BPEI] (0.30-4.0 wt%) in the fabrication process (Fig. S2b), the mass reached a plateau at ~200 °C with an additional 5-20 wt%. mass loss occurring. The shapes of these curves are consistent with the weight loss for pure GO (see ESI, Fig. S2c). On heating above 250 °C, the BPEI begins to degrade to lead to a significant mass loss between 250 °C to ~450 °C (Fig. S2c). This is consistent with the second sharp decrease in mass for the dried hydrogels (Fig. S2b). From these curves, the solid composition of GO/BPEI hydrogels is estimated from the weight loss from 250 °C to ~450 °C (BPEI mass) after subtracting the residual water (mass loss at ~120 °C). The calculated BPEI:GO mass ratio is quantified herein as *R*.

The dependence of the composition of GO/BPEI hydrogels on the batch to batch variation in GO was also determined by TGA. As shown in Fig. S2e – S2g, the dried GO/BPEI

hydrogels fabricated from different batches of GO have similar TGA curves, which suggests that they have similar compositions despite the differences in the total number of functional groups.

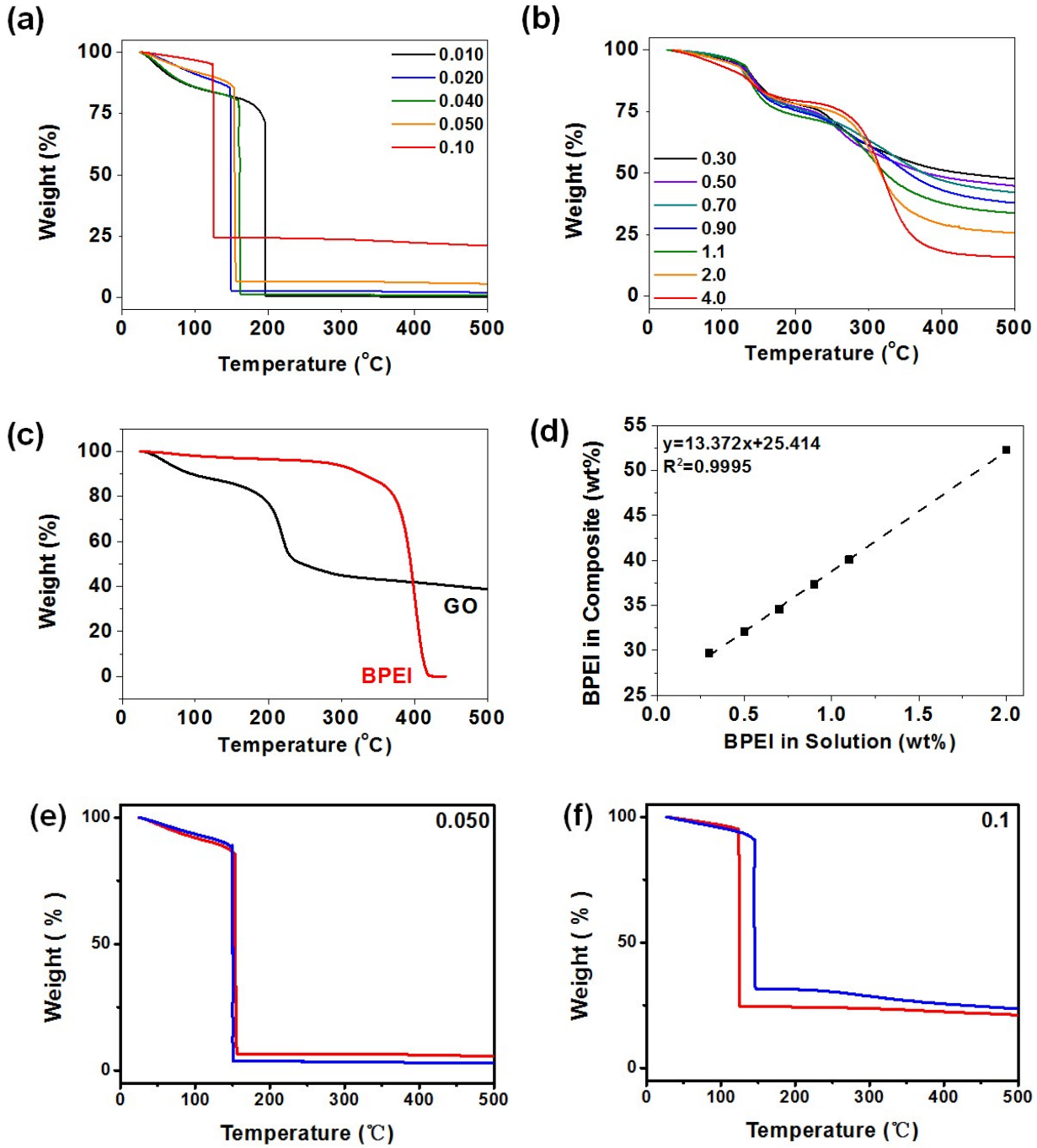

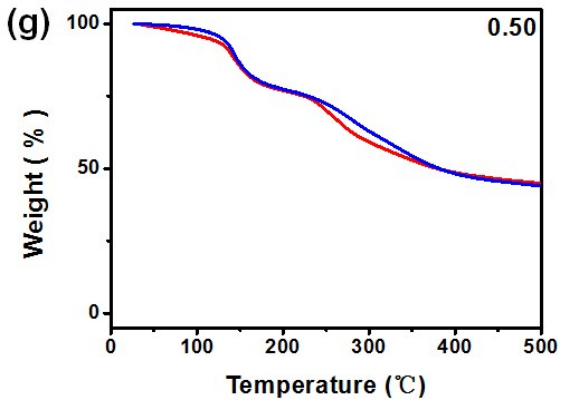

Fig. S2 (a) TGA profiles for GO and BPEI (b) TGA profiles for dried GO/BPEI hydrogels using BPEI concentrations of 0.010-0.10 wt% for the hydrogel fabrication (c) TGA profiles for dried GO/BPEI hydrogels using BPEI concentrations of 0.3-4.0 wt% for the hydrogel fabrication (d) The BPEI content in dried GO/BPEI composite with BPEI content in solution = 0.30-2.0 wt%. The dashed line is the calibration curve extrapolated from the data. The equation and the R^2 for the calibration curve are shown in the figure. (e)-(g) TGA profiles of for dried GO/BPEI hydrogels using two different batches of GO, GO - 1 (red curves) and GO – 2 (blue curves), and BPEI concentrations of 0.050-0.50 wt% for the hydrogel fabrication.

At lower [BPEI] solutions used in the fabrication, the shape of the TGA was significantly altered (Fig. S2a) where a sharp weight loss occurred at 125-200 °C. This weight loss decreased, but the initial drop occurred at lower temperatures as the BPEI concentration increased. The sharp drop is not consistent with pure GO, which suggests that the interaction between BPEI and the GO impacts the mass loss. The mass loss at low temperature (< 125 °C) for these samples (Fig. S2a) is generally larger than the nearly invariant mass loss at these temperatures for samples with higher BPEI content (Fig. S2b). In order to explain this difference, we hypothesize that there was more bounded water on the GO at low BPEI concentrations. Irrespective, this unexpected mass loss complicates the estimation of the composition for the hydrogels. Based on the higher BPEI concentrations used in the fabrication of the hydrogels in Fig. S2b (0.30 to 2.0 wt%), this BPEI concentration is linearly related to the composition of the hydrogel (Fig. S2d), which provides the basis for a calibration curve that can be applied to the hydrogels examined in Fig. S2a.

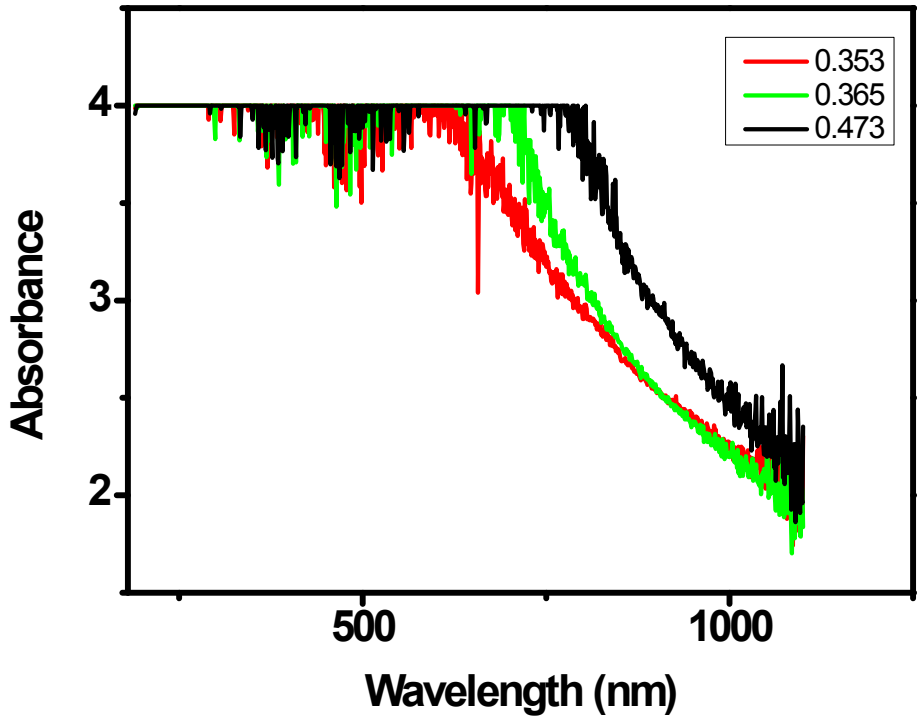

Fig. S3 UV-vis spectra of GO/BPEI hydrogels as a function of *R*. The hydrogel was placed inside of a cuvette with 1 cm path length.

Fig. S4 shows the frequency dependence of the dynamic storage modulus (*G'*) and loss modulus (*G''*) of the GO/BPEI hydrogels. Both *G'* and *G''* were nearly independent of frequency, which suggests the relaxation times of the physical crosslinks are significantly longer than the experimental time scales probed. There is a slight increase in *G'* with increasing frequency for the hydrogel; this feature presumably resulted from the imperfections in the network. The upturn of *G*'' at low frequencies suggests the beginning of the relaxation of the physical crosslinks.

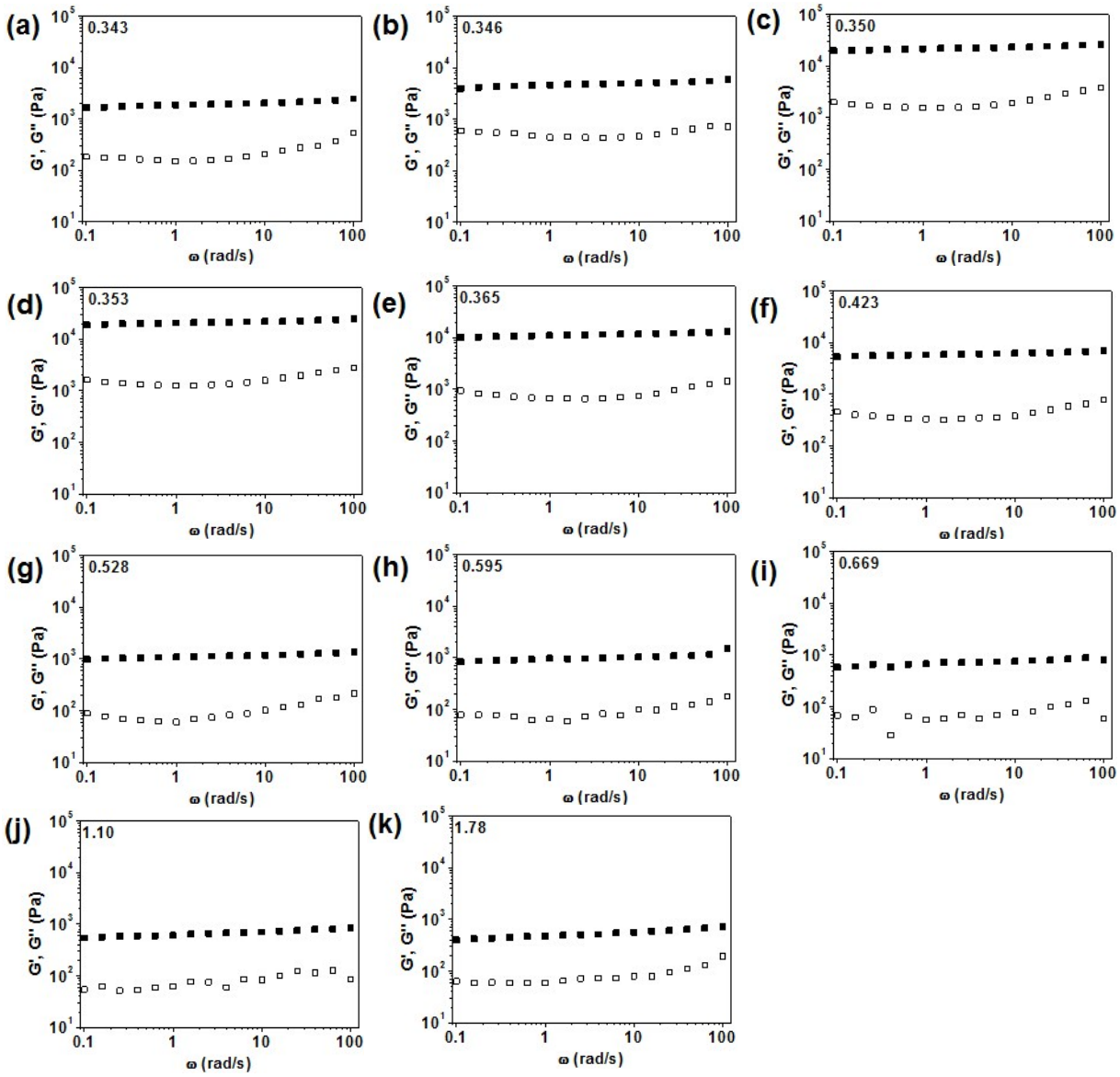

Fig. S4 The (■) storage modulus and (□) loss modulus of GO/BPEI hydrogels with *R* values from 0.343 to 1.78.

Oscillatory shear at the highest γ = 100% was applied to the hydrogels to produce a response far removed from the LVE response region. On decreasing the amplitude back to the LVE region (γ = 1%), despite the hydrogels with *R* values from 0.353 to 0.473, G_N^0s of the hydrogels only changed ~10%, which indicates that the network structure is recovered even after a large strain, Fig. S5.

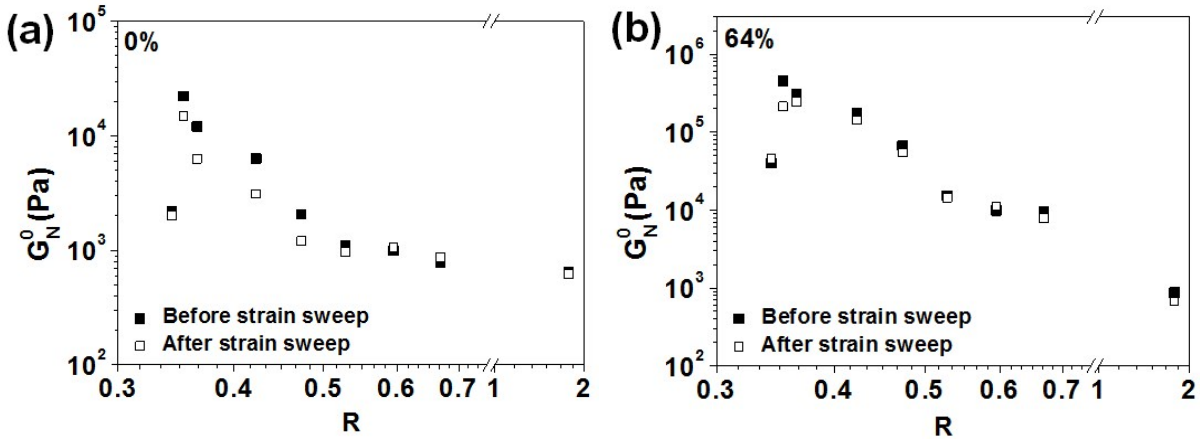

Fig. S5 The plateau modulus of the GO/BPEI hydrogel with (a) 0% and (b) 64% compressive strain at ω = 1 rad/s before and after a strain sweep with ω = 1 rad/s and γ = 0.1-100%.

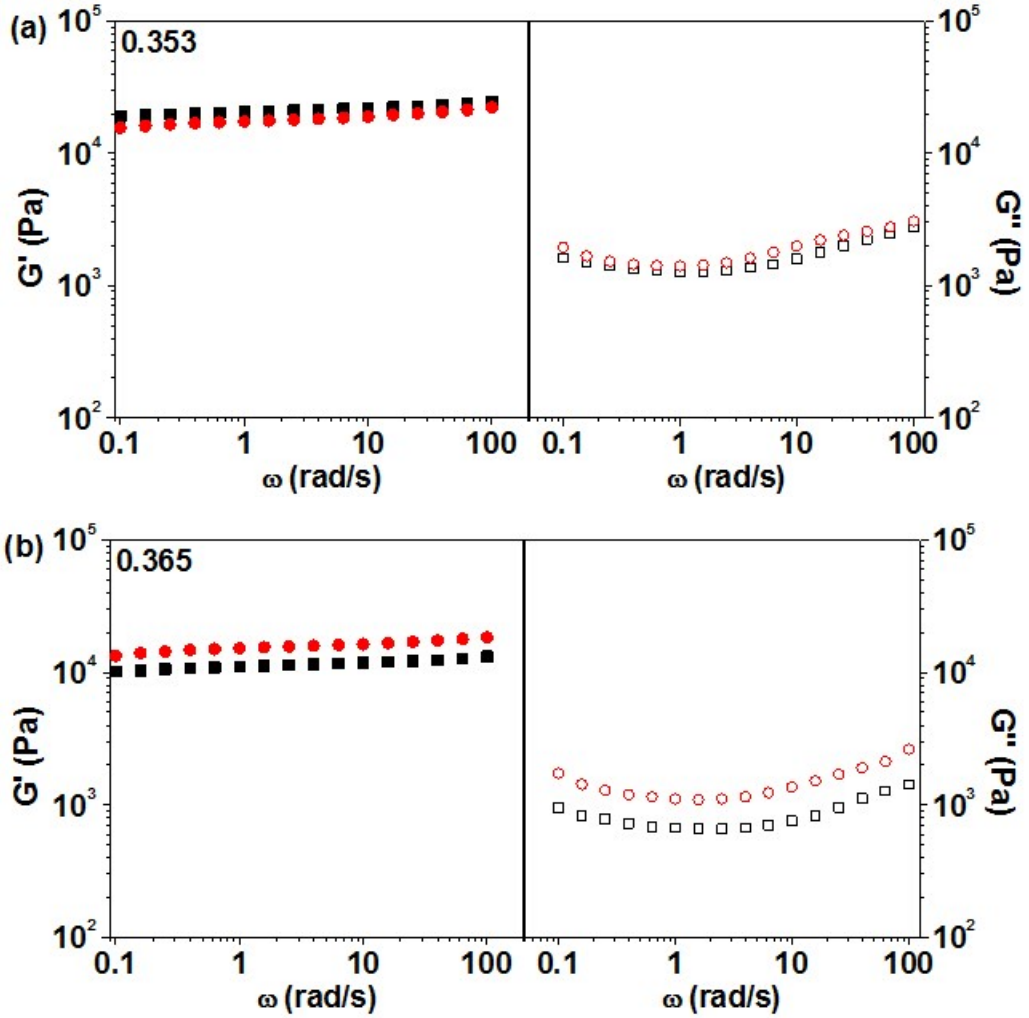

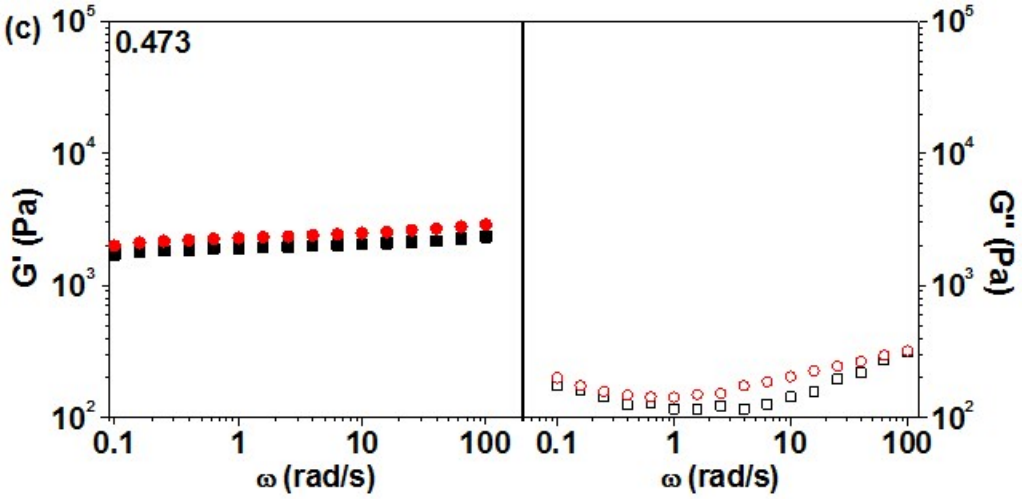

Fig. S6 The G' (solid symbols) and G'' (open symbols) of GO/BPEI hydrogels fabricated using two different batches of GO, GO - 1 (■, □) and GO – 2 (●, ○), and *R* values from 0.353 to 0.473 for the hydrogel fabrication.

Fig. S7 shows the stress relaxation responses of GO/BPEI hydrogels. After the step strain (1%), about 40% of the stress initially relaxes rapidly in ~30 s, but further relaxation of the stress is slow and continues to relax for more than 20 min. The stress relaxation behavior is qualitatively similar for all of the GO/BPEI hydrogels as shown in Fig. S7.

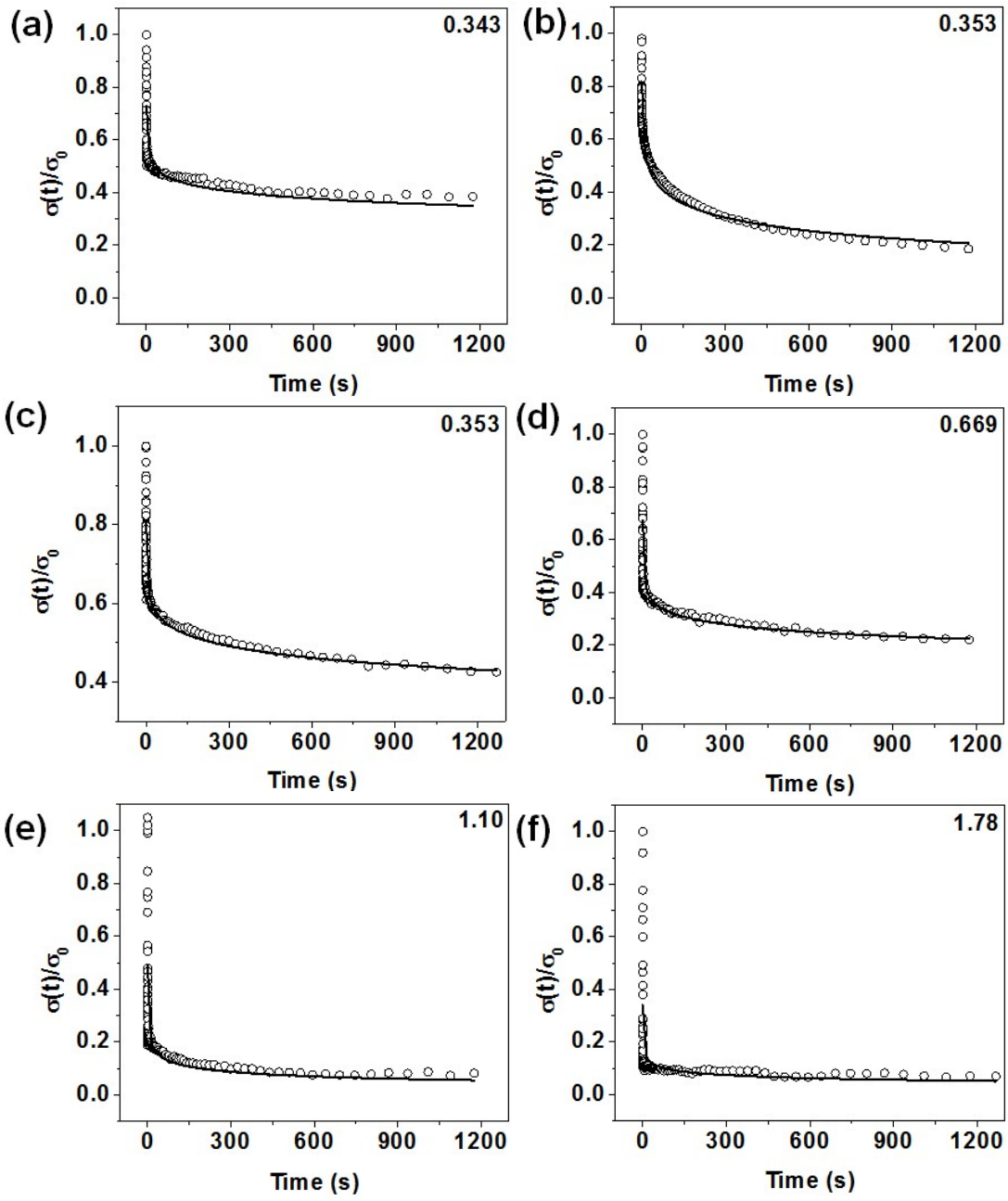

Fig. S7 The stress relaxation responses (open circle) of GO/BPEI hydrogels with *R* values from 0.343 to 1.78. The solid curves are the stretched exponential model fits.

Fig. S8 shows the average relaxation time, λ, increases with increasing R for R ≤ 0.353. At larger R, λ decreases with increasing R. When R is increased from 0.343 to 0.353, a higher density of physical crosslinks is present, requiring longer relaxation times associated with the higher λ. The increasing β with increasing R, Fig. S8, suggests a wider distribution of relaxation

times due to the existence of physical crosslinks with both long and short relaxation times. When R > 0.353, the precipitation of GO hinders the crosslinking of BPEI and GO, which weakens the hydrogel network. This impact on the network leads to faster relaxation as evidenced by the smaller λ. As short relaxation times dominates with increasing R, the distribution of relaxation times narrows (decreased β).

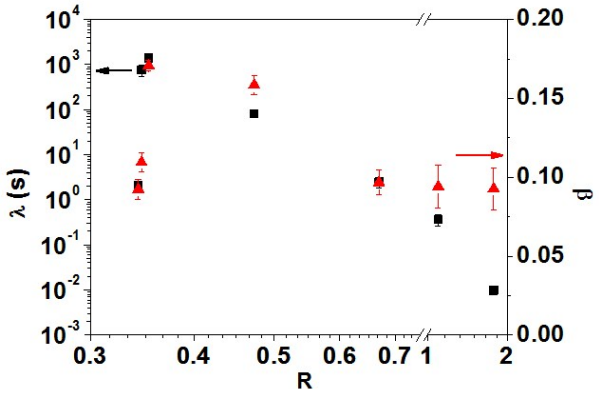

Fig. S8 The (■) average relaxation times and (▲) its distribution (β values) for GO/BPEI hydrogels as determined from the best fit of the stress relaxation with a stretched exponential.

Fig. S9 shows the long-term performance of GO/BPEI hydrogels with R = 0.353 and 0.473. As the GO/BPEI hydrogels are composed of networks of transient physical crosslinks, the hydrogel in an excess of water may not be stable if the BPEI and GO can be redispersed. For R = 0.353 and 0.473, the color of both hydrogels change from brown to black as the hydrogel ages in an excess of deionized (DI) water. This color change was potentially due to the reduction of GO by the amine groups in BPEI.[5] When R = 0.353, the swelling ratio, q, after 28 days is almost unchanged, but the plateau modulus decreased from ~23 kPa to ~15kPa, Fig. S9. When R = 0.473, there are more fluctuations in q, but q remains unchanged within experimental error. The plateau modulus for a hydrogel with R = 0.473 increases from 8.0 kPa to 14 kPa in the first two days, but then decreases to 4.0 kPa after one month. The decrease in plateau modulus of both

hydrogels suggests the weakening of physical crosslinks and the decrease in the crosslink density of the hydrogels. This conclusion is supported by the decrease in tan δ at ω = 0.1 and 100 rad/s, Fig. S10, over the same time period. A small fraction of the BPEI can be leached from the hydrogel, as confirmed by UV-vis spectroscopy (Fig. S11), which may explain this decrease in modulus. At high BPEI content (R = 1.78), the hydrogel material can be redispersed after exposure to an excess of DI water for 24 h, Fig. S12.

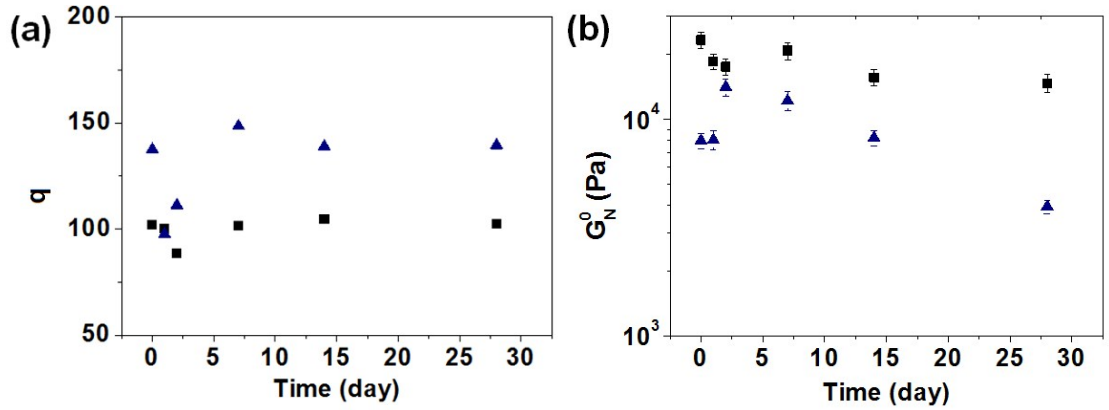

Fig. S9 The properties of the GO/BPEI hydrogels with *R* = (■) 0.353 and (▲) 0.473 were periodically over the course of one month in terms of (a) swelling ratio and (b) plateau modulus. The aging was carried out at room temperature in an excess of deionized (DI) water.

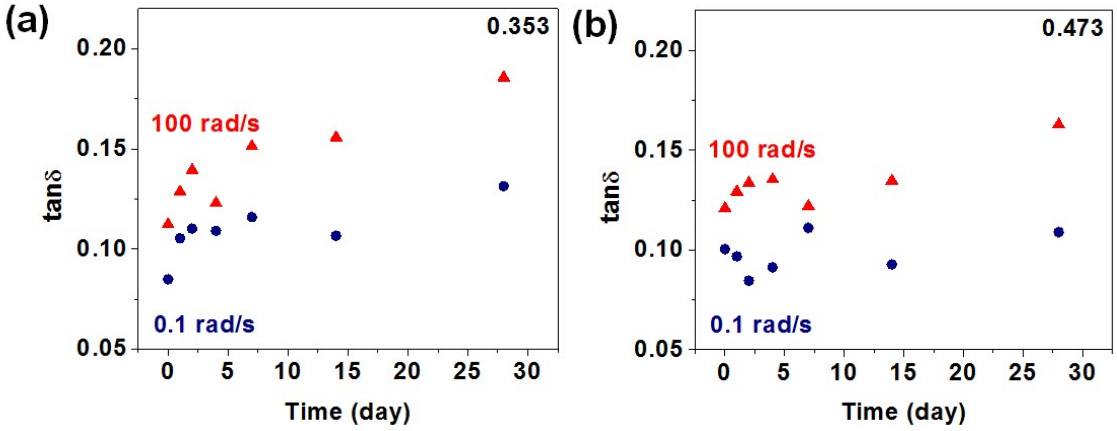

Fig. S10 The tanδ at ω = (●) 0.1 rad/s and (▲) 100 rad/s of the GO/BPEI hydrogels with (a) *R* = 0.353 and (b) *R* = 0.473 were periodically examined through the aging process at room temperature in deionized water.

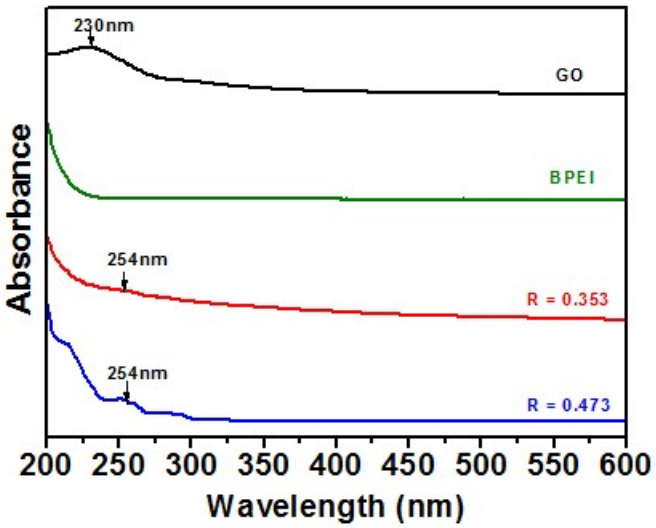

Fig. S11 The UV-vis spectra of GO/water suspension, BPEI/water solution and the Milli-Q water used for the aging of the hydrogel with R = 0.353 and 0.473 for 28 days. For GO, a π-π* plasmon peak was observed at a wavelength of 230 nm.[6] For BPEI, a broad adsorption was found at wavelengths from 200 nm to 230 nm, which possibly result from the n→σ* plasmon peak from the -NH_2 chromephore.[7] For the Milli-Q water used for aging, the broad adsorption at 200-230 nm was observed, which hinted the dissolution of BPEI in the water. Also, a peak was observed at ~254 nm for the Milli-Q water samples, which may be attributed to GO in the water that was reduced by BPEI.[8]

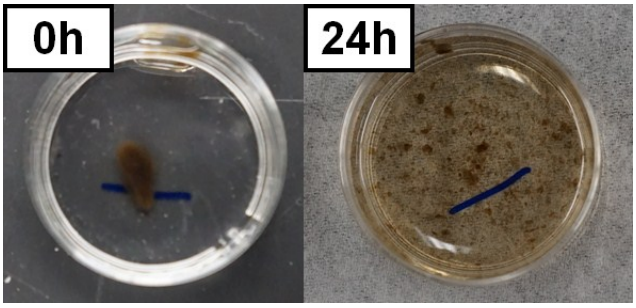

Fig. S12 GO/BPEI hydrogel with R = 1.78 immersed in excess amount of deionized water for 0 h (as-immersed) and 24 h.

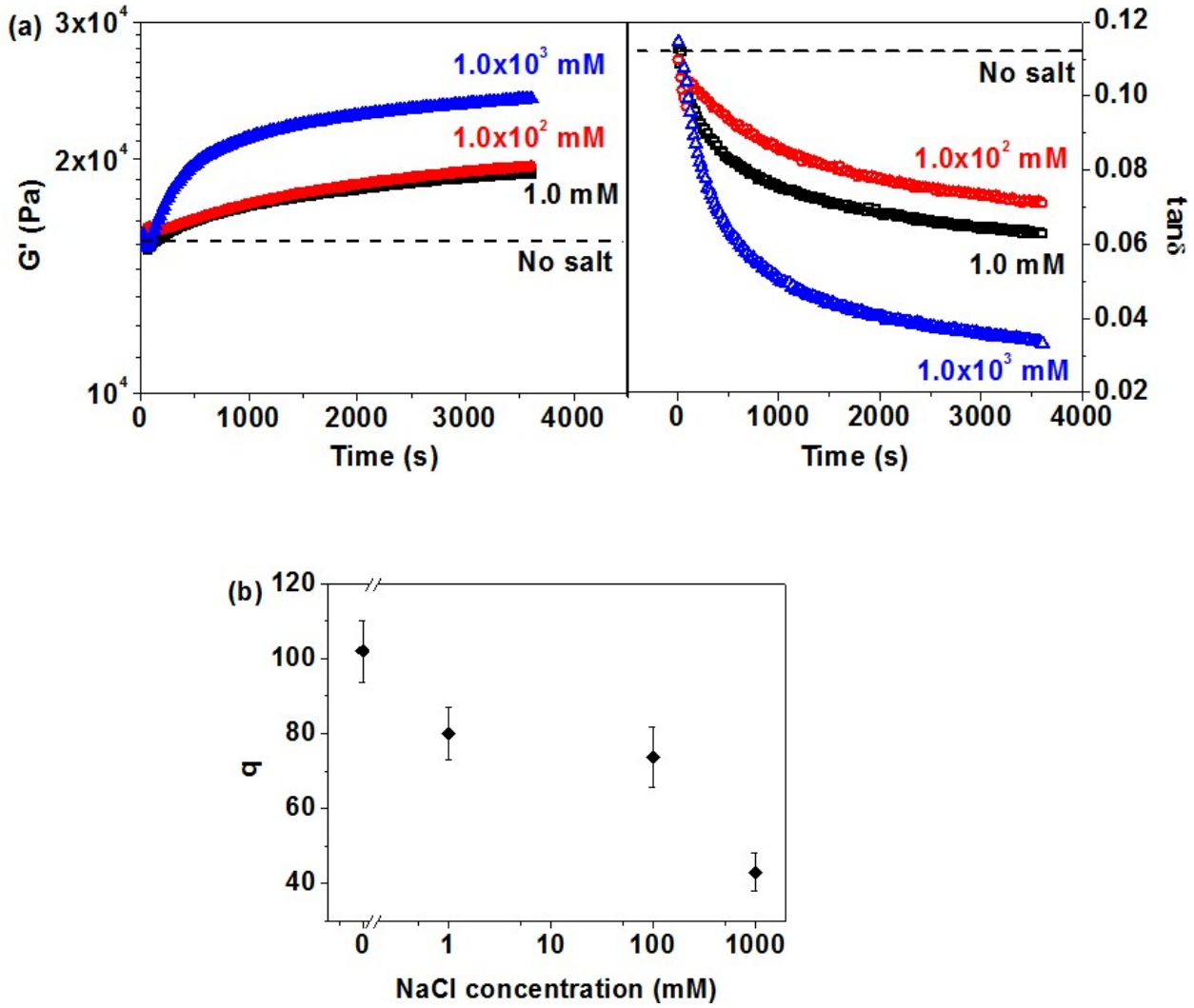

Fig. S13 (a) G' at 1 rad/s (solid symbols) and tanδ (open symbols) and (b) swelling ratios of GO/BPEI hydrogels soaked in 1.0 mM, 1.0×10^2 mM and 1.0×10^3 mM NaCl solution for 1 h. In (a), the symbols for each NaCl solutions are (■, □) 1.0 mM, (●, ○) 1.0×10^2 mM and (▲, △) 1.0×10^3 mM. The dashed lines represent average values for the no salt case.

If the 3D network in GO/BPEI hydrogels is considered as a phantom network, then the elastic shear modulus $G \sim G_N^0$ can be related to the crosslink density υ_e by Equation (5).

$$G = \upsilon_e\left(1 - \frac{2}{f}\right)\bar{R}T\upsilon_2^{2/3} \quad (5)$$

where f is the functionality of the physical crosslinks, $\bar{R}$ is the gas constant, T is the absolute temperature, and υ_2, the volume fraction of the polymer phase in the hydrogel, can be calculated by Equation (6).

$$\upsilon_2 = \left[1 + \frac{(S-1)\rho}{d}\right]^{-1} \tag{6}$$

where ρ is the density of the polymer, and d is the density of the solvent. If assumption was made that the functionality and the density of the polymer were constant during compression, the plateau modulus of the hydrogel without change in the crosslink density can be calculated from the swelling ratio change, Fig. S14f. Here, the calculated plateau moduli were way smaller than the actual ones, which suggests that the crosslink density of the hydrogels increased during compression.

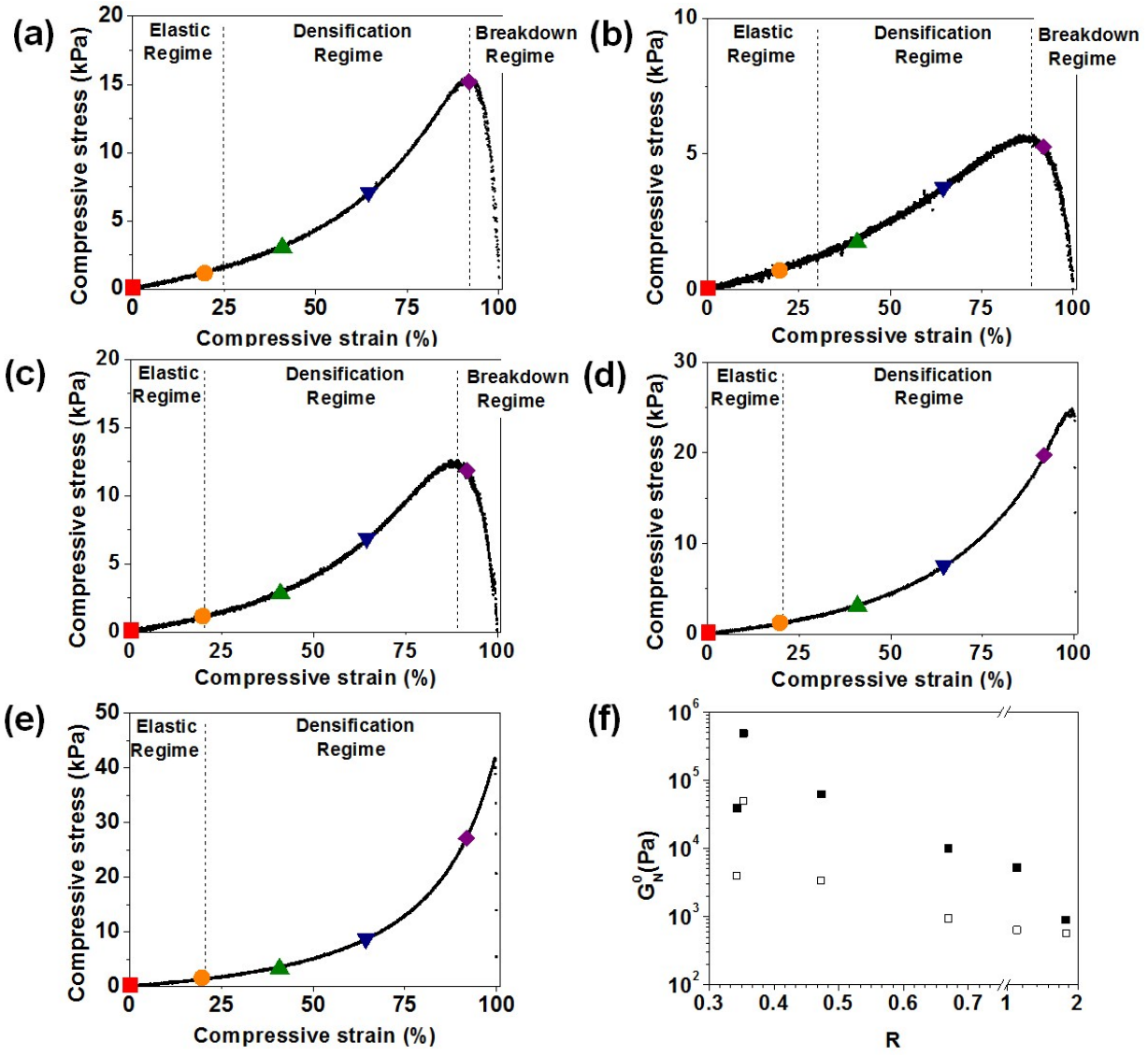

Fig. S14 (a)-(e) The typical compression curves of GO/BPEI hydrogels with *R* values of (a) 0.343 (b) 0.353 (c) 0.669 (d) 1.10 and (e) 1.78. For all the figures, the symbols for different compressive strains are (■) 0%, (●) 20%, (▲) 40%, (▼) 64% and (◆) 90%. (f) the plateau modulus from rheology tests (solid symbols) and calculations by the phantom network model (open symbol) of GO/BPEI hydrogels with *R* values from 0.343 to 1.78.

With increasing compressive strains, Fig. S15a, the GO/BPEI hydrogels show stiffening in response to the mechanical load, wherein the plateau modulus increases by 1-3 orders of magnitude. The relation between plateau modulus vs *R* remains non-monotonic under compression. The swelling ratios of the hydrogels decreased with increasing compressive strain, Fig. S15b. The extent of the decrease in the swelling ratio changed with *R*. The decrease in tan δ,

Fig. S15c, means less energy is dissipated. A calculation of the plateau moduli of the hydrogels based on phantom network theory (details discussed previously in ESI) when assuming no crosslink density change consistently result in lower moduli than measured, Fig. S14f. This calculation supports the hypothesis of an increase in the crosslink density with applied compressive strain.

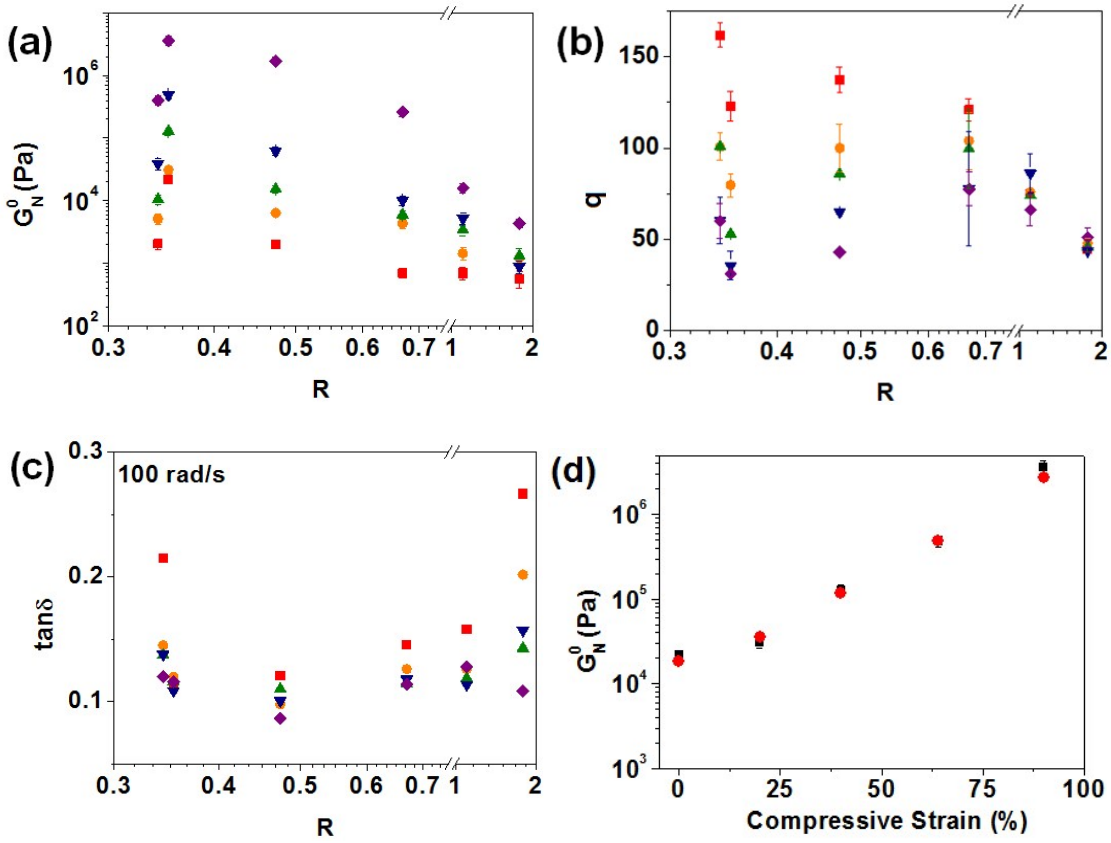

Fig. S15. (a) The R dependence of the plateau modulus of GO/BPEI hydrogels with different compressive strains. (b) The swelling ratio of the GO/BPEI hydrogels with different compressive strains. (c) The R dependence of the tanδ of GO/BPEI hydrogels at ω = 100 rad/s with different compressive strains. For all the figures, the symbols for different compressive strains are: (■) 0%, (●) 20%, (▲) 40%, (▼) 64% and (◆) 90%. (d) The compressive strain dependence of the plateau modulus of GO/BPEI hydrogels with R = 0.353 fabricated using two different batches of GO, GO - 1 (□) and GO – 2 (●).

The long-term stability of a hydrogel with R = 0.353 having been exposed to 64% compressive strain was examined, Fig. S16, by exposure to an excess of DI water. The swelling ratio

increased ~5.6% over 28 days while the plateau modulus decreased ~6% in 14 days and ~40% in 28 days. The decrease in the plateau modulus over time may due to the weakened physical crosslinks and decreased the crosslink density from leaching of a small fraction of BPEI.

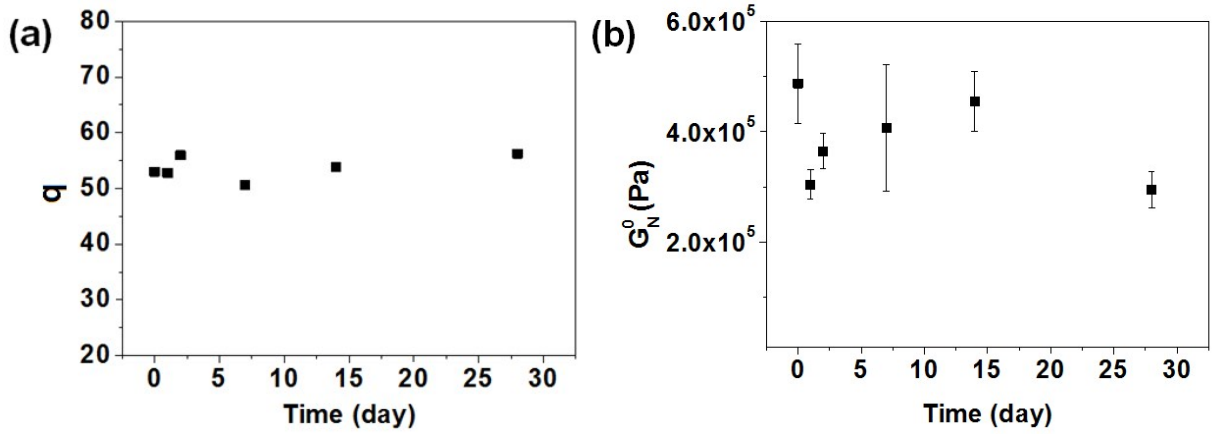

Fig. S16. (a) Swelling ratio and (b) plateau modulus of GO/BPEI hydrogels made from BPEI solution with R = 0.353, compressed to 64% strain and then kept in 10ml deionized water for different times.

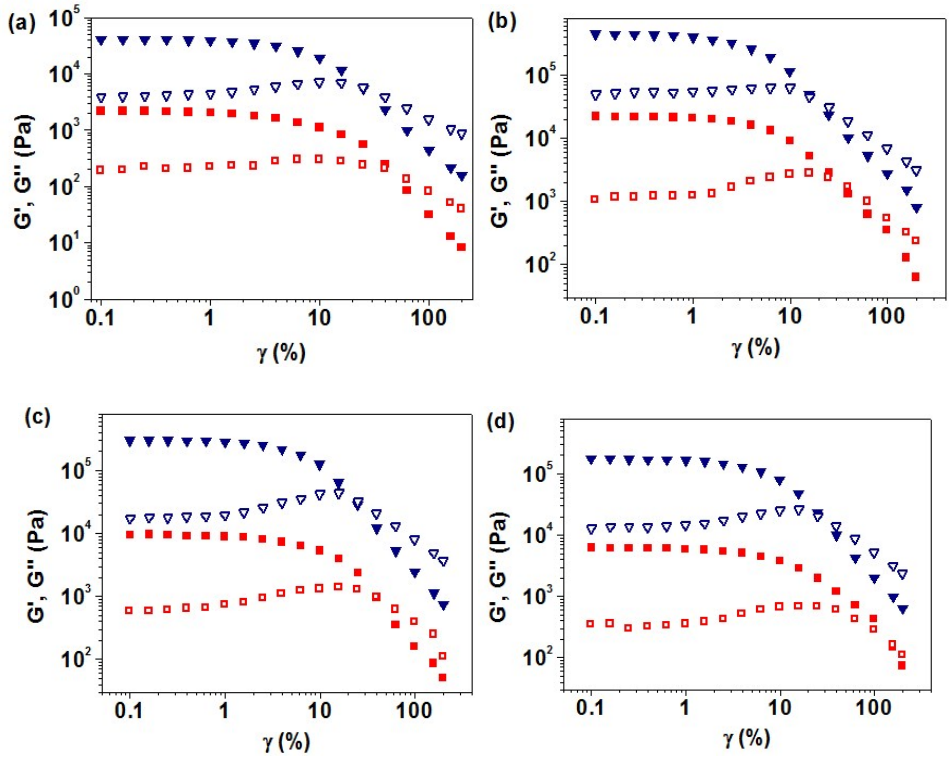

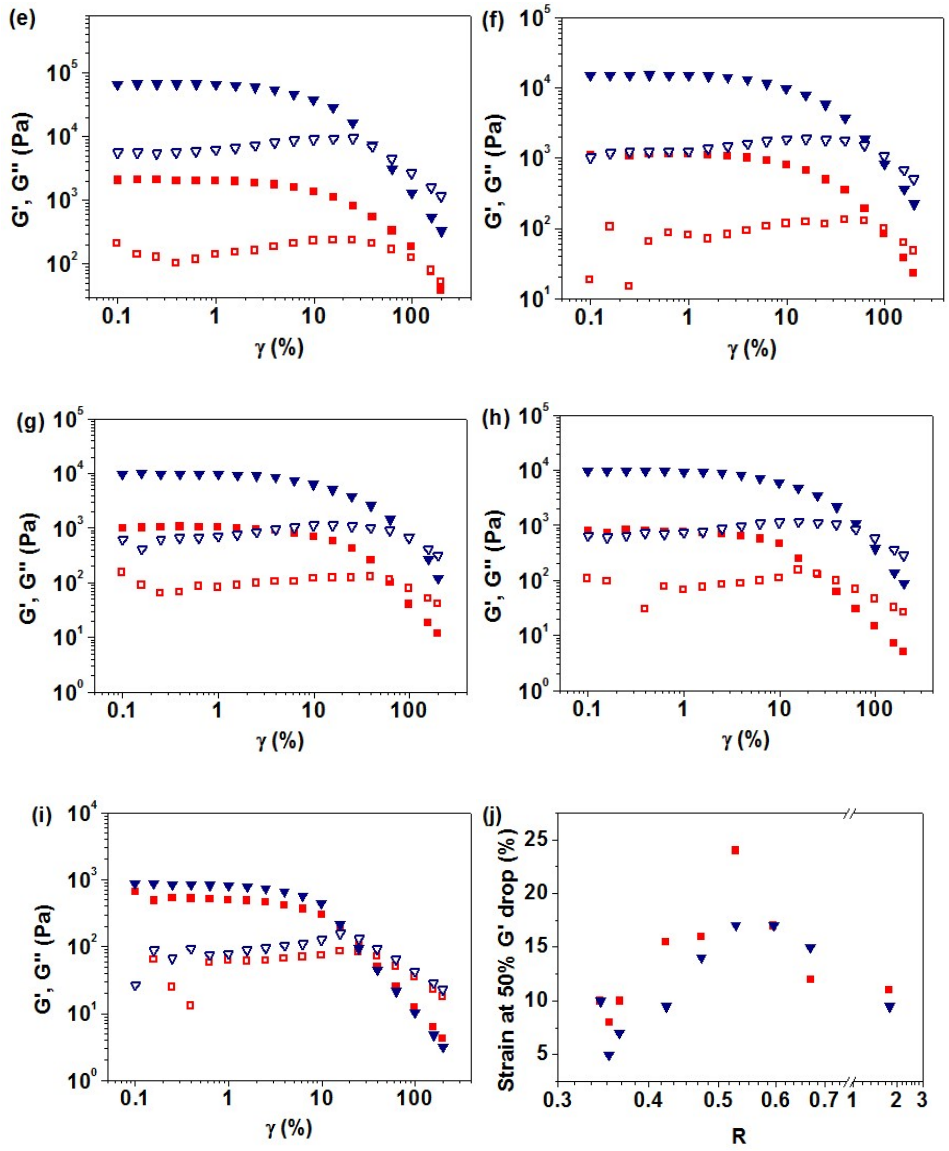

Fig. S17. Oscillatory strain dependence of G' (solid symbol) and G'' (open symbol) at (■, □) 0% and (▼, ▽) 64% compressive strains for *R* of (a) 0.343, (b) 0.353, (c) 0.365, (d) 0.423, (e) 0.473, (f) 0.528, (g) 0.595, (h) 0.669 (i) 1.78. (j) The strain at 50% drop in G' at (■) 0% and (▼) 64% compressive strains.

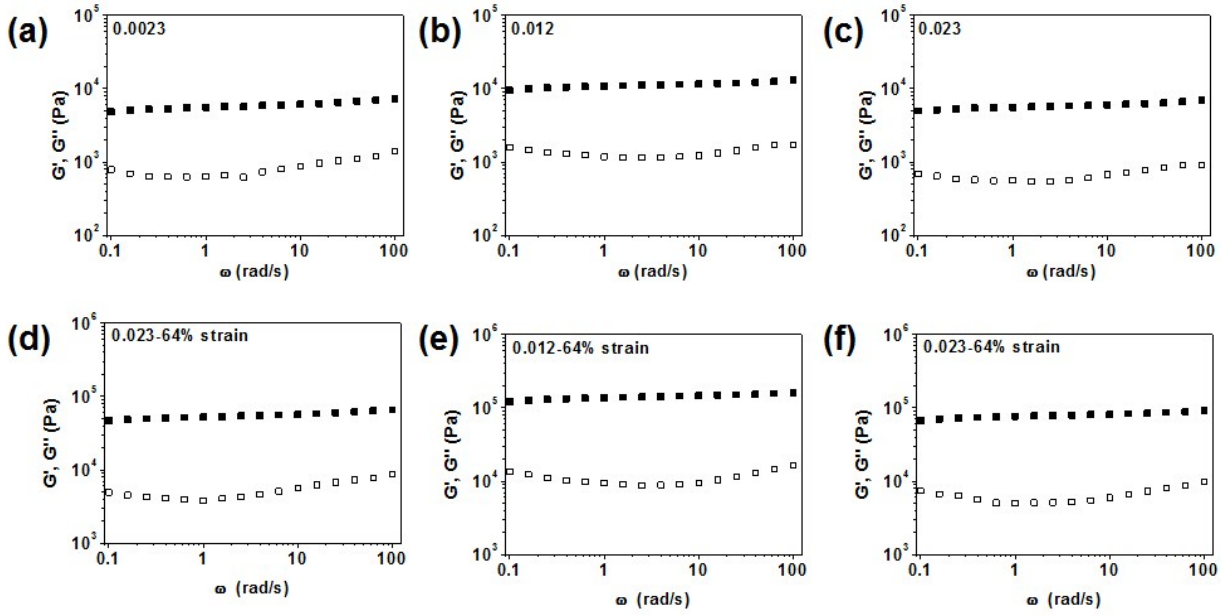

Fig. S18 The (■) storage modulus and (□) loss modulus of GO/LPEI hydrogels. (a)-(c) Hydrogels with no compressive strain. (d)-(f) Hydrogels with 64% compressive strain. The amino group concentrations in LPEI solutions are shown in the figures.

For all the dried cloisite/BPEI hydrogel samples, there was a 2-12% weight loss due to the removal of the unbounded water on BPEI. From 120 to 500 °C, the weight loss for cloisite Na^+ was negligible (~2%). The weight loss from 250 to ~ 450 °C for the cloisite/BPEI hydrogels can thus be considered from BPEI only. The solid composition of cloisite/BPEI hydrogels was estimated from the weight loss from 250 °C to ~ 450 °C (BPEI mass) after subtracting the residual water (mass loss at ~ 120 °C).

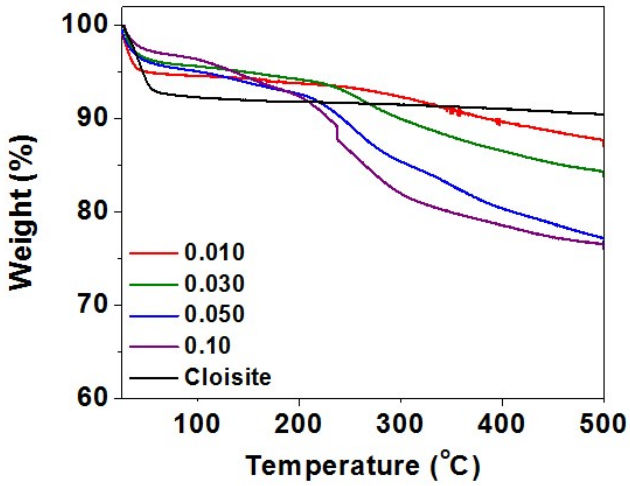

Fig. S19 TGA profiles for cloisite and dried cloisite/BPEI hydrogels using BPEI concentrations of 0.010 – 0.10 wt% for the hydrogel fabrication.

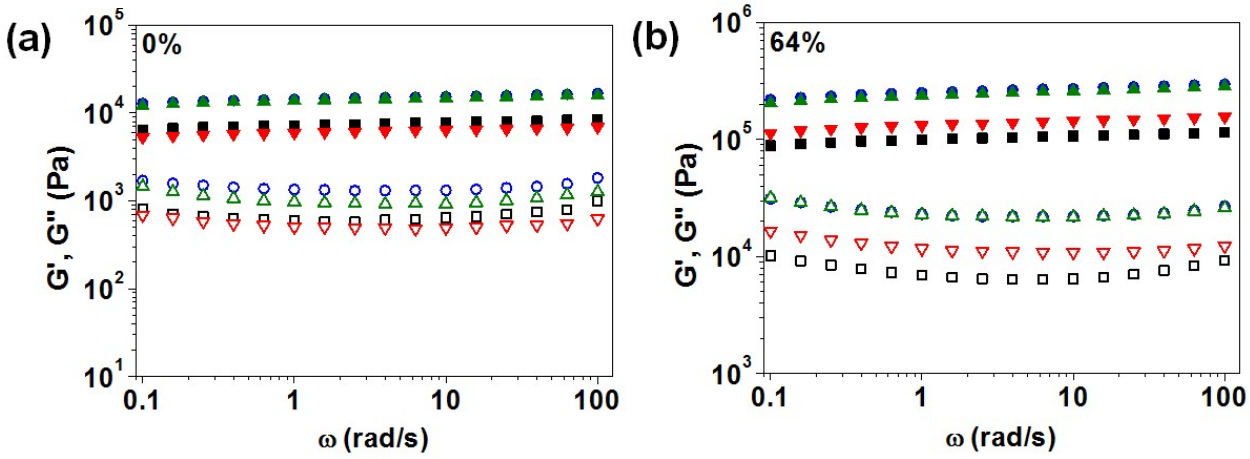

Fig. S20 The *G'* (solid symbol) and *G''* (open symbol) of cloisite/BPEI hydrogels with *R* = (■) 0.0518, (●) 0.0835, (▲) 0.123 and (▼) 0.140 wt%.

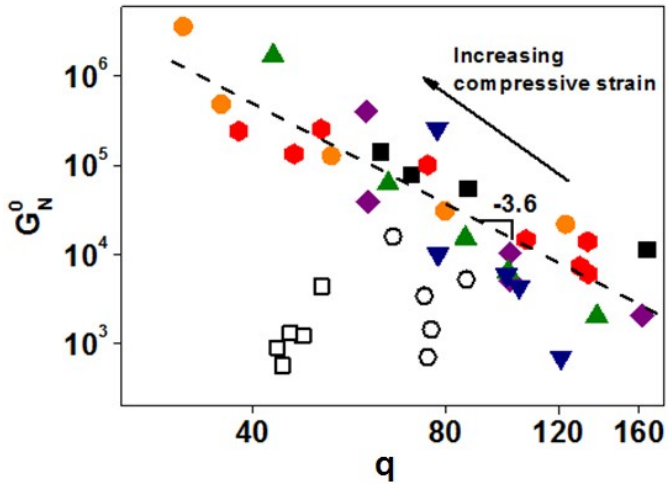

Fig. S21 Relationship between the plateau modulus and swelling ratio at different compressive strains for the (□) GO/LPEI hydrogels, (□) cloisite/BPEI hydrogels and GO/BPEI hydrogels with R = (◆) 0.343, (●) 0.353, (▲) 0.473 (▼) 0.669, (○) 1.1, and (□) 1.78.

References

1. G. Gran, *Acta Chem. Scand.*, 1950, **4**, 559-577.
2. X. Ren, J. Li, X. Tan and X. Wang, *Dalton Trans.*, 2013, **42**, 5266-5274.
3. J. Ederer, P. Janoš, P. Ecorchard, V. Štengl, Z. Bělčická, M. Šťastný, O. Pop-Georgievski and V. Dohnal, *React. Funct. Polym.*, 2016, **103**, 44-53.
4. Y. Q. Gu, X. Y. Huang, C. G. Wiener, B. D. Vogt and N. S. Zacharia, *ACS App. Mater. Interfaces*, 2015, **7**, 1848-1858.
5. D. R. Dreyer, S. Park, C. W. Bielawski and R. S. Ruoff, *Chem. Soc. Rev.*, 2010, **39**, 228-240.
6. Q. Lai, S. Zhu, X. Luo, M. Zou and S. Huang, *AIP Adv.*, 2012, **2**, 032146.
7. K. Hirayama, *Handbook of Ultraviolet and Visible Absorption Spectra of Organic Compounds* Plenum Press, New York, 1967.
8. X. Zhou, Z. Chen, D. Yan and H. Lu, *J. Mater. Chem.*, 2012, **22**, 13506-13516.